Investigation of Al-20Sn-10Cu alloy directional solidification by laboratory X-radiography

G Reinhart, F Ngomesse, F. Bertelli, P Benigni, A Campos, H Nguyen-Thi

Investigation of Al-20Sn-10Cu alloy directional solidification by laboratory X-radiography

G Reinhart[1], F Ngomesse[1], F. Bertelli[2], P Benigni[1], A Campos[3], and H Nguyen-Thi[1]

[1] Aix-Marseille Univ, Université de Toulon, CNRS, IM2NP UMR 7334, 13397 Marseille, France
[2] Sea Science Department, Federal University of São Paulo – UNIFESP, 11030-400 Santos, SP, Brazil
[3] Aix Marseille Univ, CNRS, Centrale Marseille, FSCM (FR1739), CP2M, 13397 Marseille, France

Abstract. Al-based alloys with a soft phase such as Sn are extensively used for bearing components due to their self-lubricating properties. Al-Sn alloys lack the ability to support heavy loads so the alloying with Cu as a third element provides solution strengthening of the aluminium matrix. A crucial issue in the manufacturing of Al-Sn-Cu alloys is the miscibility gap in the phase diagram of the system. Liquid immiscibility is responsible for severe segregation during the solidification process, due to the large density difference between the Al-rich and Sn-rich liquids, which limits their utilization in industry. It is therefore both scientifically and technically important to accurately understand their solidification path. In the present work, the solidification of a ternary Al-20wt.%Sn-10wt.%Cu alloys was investigated in-situ by using X-radiography. Directional solidification experiments were performed on sheet-like samples in the laboratory device SFINX (Solidification Furnace with IN-situ X-radiography), which consists of a Bridgman-type gradient furnace and an X-radiography system. The solidification sequence was determined based on the observation of the recorded images, enlightening the successive steps of the solidification path. These observations were compared to predictions obtained from thermodynamic calculations. Complementary post-mortem microscopic analyses showed that the dendrite primary trunk and secondary arms developed along <110> crystallographic axes instead of the usually expected <100>.

1. Introduction

The mechanical properties of a bearing material are a balance between a high strength for load bearing and resistance to fatigue, and a low friction coefficient for tribological applications [1]. Aluminium-tin based alloys are suitable for such applications because the presence of Sn as a soft additive provides good anti-frictional and self-lubricating properties. In addition, the alloying with a third element such as Cu can provide solid solution strengthening of the Aluminium matrix [2]. Besides the chemical composition, the microstructure forming during the solidification phase is an important feature, especially relevant for intimate surface contact where the use of lubricants is not possible [3]. A key issue in the processing of Al-Sn-Cu alloys is the liquid miscibility gap in the system, which causes the

parent liquid to decompose into two distinct immiscible liquid phases during cooling. This phase separation occurring in immiscible alloys leads to severe segregation at the microstructure level, due to the large density difference between the liquid phases that causes droplets to sink or float [4,5]. The liquid droplets can also grow and coarsen by solute diffusion or be transported by convective flows in the melt which can increase even more the detrimental impact of segregation. Research under microgravity conditions has also demonstrated that significant droplet migration is induced by thermocapillary (Marangoni) motion in the presence of a temperature gradient [6,7].

It is now well established that in-situ and time-resolved X-radiography is a method of choice for unveiling the dynamical evolution of dendritic microstructures and grain structure formation during the solidification of metal alloys [8]. However, studies of immiscible alloy solidification using this powerful observation technique are hitherto very scarce. First investigations have been carried out using synchrotron radiation sources. For example, Schaffer *et al.* investigated spinodal decomposition in hyper-monotectic Al-Bi and Al-Bi-Zn alloy [9] and highlighted the complex interactions between droplets. Lu *et al.* also studied liquid phase separation and the impact of bubbles on the segregation in Al-Bi alloys [10]. Recently, new opportunities have arisen with the improvement of compact micro-focus sources and X-ray sensitive detectors that enable *in-situ* and time-resolved radiography to be used in laboratory devices, with a sufficient spatial and time resolutions to distinguish the microstructure features [11], enabling different orientations of the sample with respect to gravity [12] and compatible with microgravity platforms [13,14]. Such a laboratory device was successfully used by Xavier *et al.* to analyse the morphology of the solidification interface at different cooling rates for an Al-Bi-Cu monotectic alloy [15].

The present work reports on the solidification of an Al-20wt.%Sn-10wt.%Cu sample observed *in situ* using the SFINX (Solidification Furnace with IN-situ X-radiography) laboratory device. The solidification sequence will be described based on the observation of the recorded images. These observations will be compared to predictions obtained from thermodynamic calculations. Complementary post-mortem microscopic analyses will be used to determine the growth orientation of the dendrite primary trunk and secondary arms.

2. Experimental details

The SFINX facility available at IM2NP laboratory was used and was described in detail in [16]. It has been developed within the framework of the ESA MAP named XRMON (In-situ X-ray monitoring of advanced metallurgical processes under microgravity and terrestrial conditions), devoted to the application of X-radiography during microgravity experiments [17]. The core of the facility is a solidification furnace consisting of two heaters separated by a gap that applies a longitudinal temperature gradient G_{app}. The gradient furnace enables directional solidification with cooling rates R within the range of 0.01–1.5 K/s and applied temperature gradient within the range of 5–15 K/mm.

The X-radiography system figures a micro-focus X-ray source with a molybdenum target (3 μm focal spot) providing enough photon flux and has two peaks of energy 17.4 keV and 19.6 keV ensuring a good image contrast to study Al–Cu based alloys. The camera system consists of a scintillator plate and a digital camera with a CCD-sensor. Due to the beam divergence, a geometric magnification of the object is observed at the detector, corresponding to the ratio of the source-detector by source-sample distances. Here, a magnification of approximately 5 was used for a Field-of-View (FoV) of about 5 × 5 mm^2 leading to an effective pixel size of approximately 4 μm. The acquisition rate was 2 frames per second. The studied alloy was Al-20wt.%Sn-10wt.%Cu. The three elements have significantly different absorption contrast so that the liquid and solid phases that are expected to form during the solidification sequence will be clearly distinguishable. Sheet-like rectangular sample of 5 mm × 50 mm in area and about 250 μm in thickness were used. The sample was placed in the middle of stainless-steel spacers sandwiched between two glassy carbon sheets sewn together with a silica thread. The crucible was inserted inside the furnace and meets both sides to achieve the expected thermal profile. The furnace

was set in vertical position, with the sample length parallel to the gravity vector **g**. This configuration is chosen to highlight gravity-related phenomena such as buoyancy.
The X-radiography system recorded a stack of raw images during the sample solidification. The grey level variations in the recorded images are related to the attenuation coefficient of each different part of the sample. Image legibility is enhanced by applying a "flat-field" correction, which consists in dividing each frame by a reference image recorded just before solidification. This procedure reduces the noise and removes defects related to the detector and crucible [18]. After applying the image processing, the bright regions in the processed radiograph are solid Al-grains whereas the dark regions are the Cu-rich and/or Sn-rich liquid regions.

3. Results and discussion

In the present study, we will consider an experiment carried out with a cooling rate, R = 0.45 K/s, and an applied temperature gradient G_{app} = 5.5 K/mm. These parameters were chosen to obtain a microstructure with features (dendrite arm spacing, interdendritic liquid fraction) that are distinguishable with respect to the spatial resolution.

3.1. Theoretical solidification sequence

The solidification paths of hypo-eutectic binary Al-Cu and Al-Sn alloys are rather standard with the formation of aluminium as primary phase and then of eutectic from the residual liquid. However, the comprehension of the solidification path in the ternary Al-Cu-Sn system is more complex, in part due to the presence of a liquid miscibility gap. In a first approach, the solidification path of the Al-20wt.%Sn-10wt.%Cu alloy has been determined by the use of the Thermo-Calc software [19] and the COST 507 database [20]. Figure 1 depicts the successive steps during cooling (from the right side to the left side) in the form of the calculated phase fraction as a function of temperature.

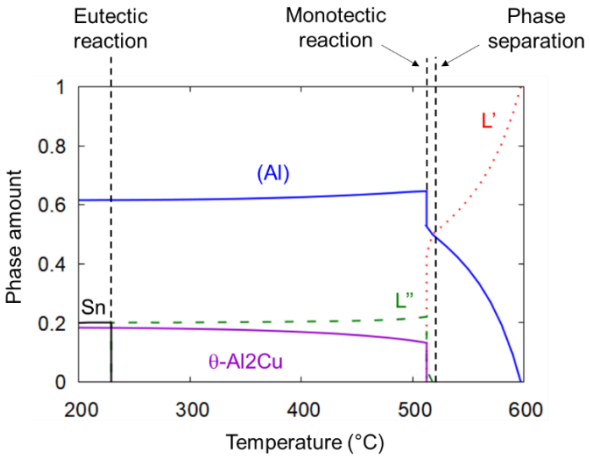

Figure 1. Thermodynamic calculation of the phase evolution during cooling in Al-20wt.%Sn-10wt.%Cu.

The predicted solidification sequence is in agreement with previous studies found in the literature [4,21] and takes place as follows. It commences with the solidification of the α-Al phase and the gradual increase of the liquid phase L′ composition in Sn and Cu due to solute rejection. When the liquid phase L' reaches the boundary of the miscibility gap, phase separation occurs with the formation of Sn-rich liquid L″. At lower temperature, the remaining liquid L′ is transformed during a monotectic reaction that induces the concomitant formation of a large quantity of α-Al and θ-Al_2Cu solid phases. Finally, the remaining liquid L″ is consumed through a eutectic reaction that forms the solid Sn phase.

3.2. In-situ observation of the solidification sequence

X-radiography has been used to visualise in-situ the solidification sequence of an Al-20wt.%Sn-10wt.%Cu sample. The sample was firstly directionally melted from the top and towards the bottom part of the sample. A smooth and planar solid-liquid interface was obtained after a stabilization time of approximately 30 minutes. Then, solidification was triggered by cooling down the two heaters. A selection of radiographs recorded during the solidification is shown in Figure 2. At first, a columnar dendritic microstructure developed (Figure 2a), which corresponds to the α-Al phase. These dendrites appear in light grey while the surrounding liquid appears darker due to the rejection of Cu and Sn solutes that have higher X-ray absorption coefficients. It is already possible to notice that secondary dendrite arms do not develop perpendicular to the primary trunks as usually expected in aluminum alloys, but with a lower angle.

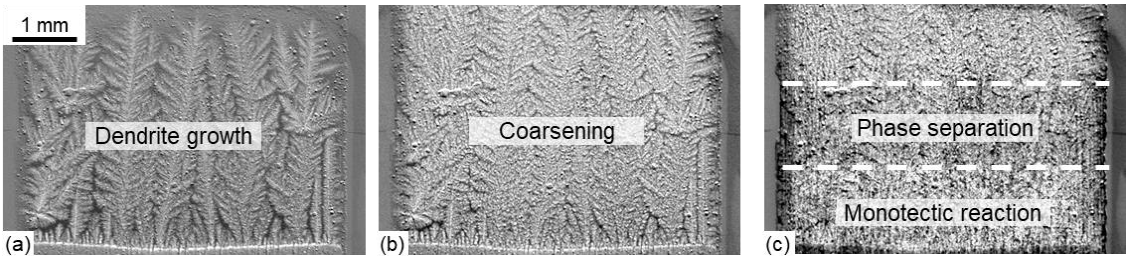

Figure 2. Sequence of radiographs showing: (a) the columnar dendritic growth ($t = t_0 + 73$ s), (b) the microstructure coarsening ($t = t_0 + 121$ s) and (c) the phase separation and monotectic reaction in the mushy zone ($t = t_0 + 162$ s). ($R = 0.45$ K/s, $G_{app} = 5.5$ K/mm).

Cooling and coarsening in the mushy zone led to the formation of thicker microstructures with time (Figure 2b). A few minutes later, the formation of a dark layer in the mushy zone is visible, that crossed the field of view from bottom to top (middle of Figure 2c). This upper boundary of the dark layer is the beginning of the liquid phase separation as expected from the theoretical solidification path, with the formation of many black droplets (a few tens of microns in size) in between the dendrites. Those droplets are Sn-rich liquid L″, having a higher X-ray absorption than the other phases. The lower boundary of the dark layer corresponds to the beginning of the monotectic reaction. During this step, a large amount of α-Al and θ-Al_2Cu are expected to form, which are mainly composed of aluminum and consequently have lower X-ray absorption coefficients. Therefore, α-Al and θ-Al_2Cu solid formations induce a brightening of the mushy zone on the radiographs. Finally, after approximately 15 minutes, the crossing of a last front induced a weak darkening of the mushy zone, unfortunately not distinguishable on static images but visible on videos. This last step of the solidification sequence is attributed to the solidification of the remaining Sn-rich liquid droplets with to the final eutectic reaction, in agreement with the theoretical solidification sequence.

3.3. Growth orientation of the dendrite arms

A careful examination of the dendrite morphology highlights that the secondary dendrite arms do not develop perpendicular to the primary trunks as usually expected in aluminium alloys, but with a lower angle (Figure 3a). The growth orientation of the dendrite arms was determined unambiguously by post-mortem analyses using EBSD (Electron Backscatter Diffraction). Orientation maps were collected using a Zeiss Gemini 500 field-emission gun scanning electron microscope (FEG-SEM) equipped with an EDAX Hikari Super acquisition system.

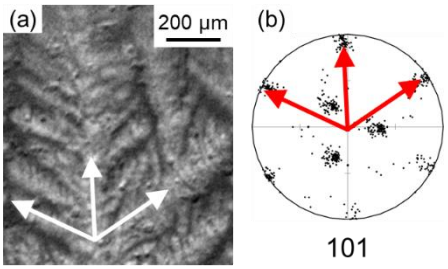

Figure 3. (a) Close-up of a radiograph showing an aluminium dendrite and (b) corresponding (101) pole figure obtained by EBSD.

The comparison between the arm growth directions (Figure 3a) and the (101) pole figure obtained for a dendritic crystal (Figure 3b) confirms that the primary trunk and secondary arms have been developing in <110> directions instead of the common <100> directions. Further experiments with various amounts of Sn and Cu are planned to determine if a dendrite orientation transition (DOT) can occur in the ternary Al-Sn-Cu system, as also reported in binary systems [22–24].

4. Conclusion

The solidification of the ternary Al-20wt.%Sn-10wt.%Cu alloy was investigated by means of in-situ X-radiography. The experimental solidification sequence agrees with calculations performed using a computational thermodynamics software. In addition, EBSD analyses showed that the dendrite arms developed along <110> crystallographic axes instead of the common <100> directions. Investigations are planned to determine how this different orientation from the standard for Al-alloys imposes trapping of tin in the form of pockets between primary and secondary dendritic arms, consequently affecting the desired properties for applications of these alloys.

Further analyses will deepen the comparison of the experimental results with the theoretical solidification path, such as the accurate determination of the phase transformation temperature by using differential scanning calorimetry (DSC). Similar investigations will also be conducted to investigate the solidification of Al-Sn-Cu alloys with various compositions and the conditions for a DOT to occur in this system. The characterisation of the droplet motion and phase distribution is also in progress.

Acknowledgement

This work is supported by the French National Space Agency (CNES). The authors would also like to thank the Swedish Space Corporation (SSC) for the development of the SFINX facility and the technical support.

References

[1] Fang X and Fan Z 2006 Rheo-diecasting of Al–Si–Pb immiscible alloys *Scr. Mater.* **54** 789–93

[2] Kong C J, Brown P D, Harris S J and McCartney D G 2005 The microstructures of a thermally sprayed and heat treated Al–20 wt.%Sn–3 wt.%Si alloy *Mater. Sci. Eng. A* **403** 205–14

[3] Bertelli F, Brito C, Ferreira I L, Reinhart G, Nguyen-Thi H, Mangelinck-Noël N, Cheung N and Garcia A 2015 Cooling thermal parameters, microstructure, segregation and hardness in directionally solidified Al–Sn-(Si;Cu) alloys *Mater. Des.* **72** 31–42

[4] Kotadia H R, Doernberg E, Patel J B, Fan Z and Schmid-Fetzer R 2009 Solidification of Al-Sn-Cu Based Immiscible Alloys under Intense Shearing *Metall. Mater. Trans. A* **40** 2202–11

[5] Kotadia H R, Das A, Doernberg E and Schmid-Fetzer R 2011 A comparative study of ternary Al–Sn–Cu immiscible alloys prepared by conventional casting and casting under high-intensity ultrasonic irradiation *Mater. Chem. Phys.* **131** 241–9

[6] Ratke L and Diefenbach S 1995 Liquid immiscible alloys *Mater. Sci. Eng. R Rep.* **15** 263–347

[7] Jiang H, Li S, Zhang L, He J and Zhao J 2019 Effect of microgravity on the solidification of aluminum–bismuth–tin immiscible alloys *Npj Microgravity* **5** 1–9

[8] Akamatsu S and Nguyen-Thi H 2016 In situ observation of solidification patterns in diffusive conditions *Acta Mater.* **108** 325–46

[9] Schaffer P L, Mathiesen R H, Arnberg L, Sabatino M D and Snigirev A 2008 In situ investigation of spinodal decomposition in hypermonotectic Al–Bi and Al–Bi–Zn alloys *New J. Phys.* **10** 053001
[10] Lu W, Zhang S, Zhang W, Kaptay G, Yu J, Fu Y and Li J 2015 Direct observation of the segregation driven by bubble evolution and liquid phase separation in Al–10 wt.% Bi immiscible alloy *Scr. Mater.* **102** 19–22
[11] Rakete C, Baumbach C, Goldschmidt A, Samberg D, Schroer C G, Breede F, Stenzel C, Zimmermann G, Pickmann C, Houltz Y, Lockowandt C, Svenonius O, Wiklund P and Mathiesen R H 2011 Compact x-ray microradiograph for in situ imaging of solidification processes: Bringing in situ x-ray micro-imaging from the synchrotron to the laboratory *Rev. Sci. Instrum.* **82** 105108
[12] Klein S, Braeuer D, Becker M, Knipstein A, Meckel S, Sondermann E and Kargl F 2016 X-RISE - A Multifunctional X-ray Radiography Device for Parabolic Flights and Laboratory Use *Int. J. Microgravity Sci. Appl.* **33** 330405
[13] Nguyen-Thi H, Reinhart G, Salloum-Abou-Jaoude G, Browne D J, Murphy A G, Houltz Y, Li J, Voss D, Verga A, Mathiesen R H and Zimmermann G 2014 XRMON-GF Experiments Devoted to the in Situ X-ray Radiographic Observation of Growth Process in Microgravity Conditions *Microgravity Sci. Technol.* **26** 37–50
[14] Ngomesse F, Reinhart G, Soltani H, Zimmermann G, Browne D J, Sillekens W and Nguyen-Thi H 2021 In situ investigation of the Columnar-to-Equiaxed Transition during directional solidification of Al–20 wt.%Cu alloys on Earth and in microgravity *Acta Mater.* **221** 117401
[15] Xavier M G C, Reyes R A V, Gomes L F, Spinelli J E, Mangelinck-Noël N, Nguyen-Thi H and Reinhart G 2020 Combined growth of α-Al and Bi in a Al-Bi-Cu monotectic alloy analyzed by in situ X-ray radiography *J. Cryst. Growth* **536** 125592
[16] Soltani H, Reinhart G, Benoudia M C, Zahzouh M and Nguyen-Thi H 2019 Impact of gravity-related phenomena on the grain structure formation: comparative study between horizontal and vertical solidification of a refined Al-20wt.%Cu alloy *IOP Conf. Ser. Mater. Sci. Eng.* **529** 012019
[17] Browne D J, Garcia-Moreno F, Nguyen-Thi H, Zimmermann G, Kargl F, Mathiesen R H, Griesche A and Minster O 2017 Overview of In Situ X-Ray Studies of Light Alloy Solidification in Microgravity *Magnesium Technology 2017* ed K N Solanki, D Orlov, A Singh and N R Neelameggham (Cham: Springer International Publishing Ag) pp 581–90
[18] Buffet A, Nguyen-Thi H, Bogno A, Schenk T, Mangelinck-Noël N, Reinhart G, Bergeon N, Billia B and Baruchel J 2010 Measurement of Solute Profiles by Means of Synchrotron X-Ray Radiography during Directional Solidification of Al-4 wt% Cu Alloys *Mater. Sci. Forum* **649** 331–6
[19] Andersson J-O, Helander T, Höglund L, Shi P and Sundman B 2002 Thermo-Calc & DICTRA, computational tools for materials science *Calphad* **26** 273–312
[20] Ansara I, Rand M and Dinsdale A 1998 COST-507 - Definition of thermochemical and thermophysical properties to provide a database for the development of new light alloys: Thermochemical database for light metal alloys vol 2 (European Commission, Directorate-General for Research and Innovation)
[21] Bertelli F, Brito C, Ferreira I L, Reinhart G, Nguyen-Thi H, Mangelinck-Noël N, Cheung N and Garcia A 2015 Cooling thermal parameters, microstructure, segregation and hardness in directionally solidified Al–Sn-(Si;Cu) alloys *Mater. Des.* **72** 31–42
[22] Gonzales F and Rappaz M 2006 Dendrite growth directions in aluminum-zinc alloys *Metall. Mater. Trans. A* **37** 2797–806
[23] Becker M, Dantzig J A, Kolbe M, Wiese S T and Kargl F 2019 Dendrite orientation transition in AlGe alloys *Acta Mater.* **165** 666–77
[24] Wang L, Hoyt J J, Wang N, Provatas N and Sinclair C W 2020 Controlling solid-liquid interfacial energy anisotropy through the isotropic liquid *Nat. Commun.* **11** 724